Grain coarsening behaviour of solution annealed Alloy 625 between 600-800°C

I. J. Moore[a,*], J. I. Taylor[a], M. W. Tracy[a], M. G. Burke[b], E. J. Palmiere[a]

[a]*Department of Materials Science and Engineering, The University of Sheffield, Sir Robert Hadfield Building, Mappin Street, Sheffield, S1 3JD, UK.*
[b]*Materials Performance Centre, The University of Manchester, The Mill, Sackville Street, Manchester, M13 9PL, UK.*

Abstract

As with all alloys, the grain structure of the nickel-base superalloy 625 has a significant impact on its mechanical properties. Predictability of the grain structure evolution in this material is particularly pertinent because it is prone to inter-metallic precipitate formation both during manufacture and long term or high temperature service. To this end, analysis has been performed on the grain structure of Alloy 625 aged isothermally at temperatures between 600-800°C for times up to 3000 hours. Fits made according to the classical Arrhenius equation describing normal grain growth yield an average value for the activation energy of a somewhat inhomogeneous grain structure above 700°C of 108.3±6.6 kJ mol^{-1} and 46.6±12.2 kJ mol^{-1} below 650°C. Linear extrapolation between 650-700°C produces a significantly higher value of 527.7 ± 23.1 kJ mol^{-1}. This result is ultimately a consequence of a high driving force, solute-impeded grain boundary migration process operating within the alloy. Comparison of the high and low temperature values with the activation energy for volume self-diffusion and grain boundary diffusion identifies the latter as the principle governing mechanism for grain growth in both instances. A decrease in the value of the time exponent (n) at higher temperatures despite a reduction in solute drag is attributable to the Zener pinning imposed by grain boundary M_6C and $M_{23}C_6$ particles identified from Transmission Electron Microscopy (TEM) and Energy Dispersive X-ray Spectroscopy (EDXS) analysis. Vickers hardness results show the dominance of intermetallic intragranular precipitates in

1

the governance of the mechanical properties of the material with grain coarsening being accompanied by a significant increase in hardness. Furthermore, the lack of any correlation with grain growth behaviour indicates these phases have no significant effect on the grain evolution of the material.

Keywords:

Grain Coarsening, Alloy 625, Vickers Hardness, Activation Energy, Precipitation, Solute Drag.

1. Introduction

Despite its price premium when compared to many other superalloys, the particularly high corrosion resistance and strength offered by Alloy 625 has resulted in its application in a number of specialist areas including petrochemicals, marine and nuclear [1, 2, 3, 4, 5, 6]. One of the key factors considered when utilising the alloy is the formation of secondary phases, particularly body-centre-tetragonal (BCT) $D0_{22}$ γ'' and $D0_a$ orthorhombic δ phase (both with the nominal composition $NbNi_3$), which have been demonstrated to have a significant impact on the mechanical properties of any component [7, 8, 9, 10]. Accordingly, almost all of the published ageing studies carried out using Alloy 625 have focused principally on the formation and evolution of these two phases and the subsequent mechanical effects thereof *viz.* a discussion of the grain behaviour is absent [11, 12, 13, 14, 15, 16, 17, 18, 19].

The effects of grain size (demonstrated to be key in governing properties such as creep resistance and strength in nickel-base superalloys [20]) are particularly significant in components constructed from Alloy 625 due to their being typically being installed in a solution annealed (precipitate free) state [21]. In this regard, therefore, given the propensity of precipitates to form in such components in high temperature service [12] alongside inevitable

*Corresponding author

Email address: `imoore1@sheffield.ac.uk` (I. J. Moore)

grain growth/coarsening, and owing to their competing effect on mechanical properties, the absence of a detailed study in the literature regarding their effect on Alloy 625 grain growth constitutes a significant omission. This eventuality is particularly significant given the con-

20 struction of a coherent (over a range of temperatures) description for Alloy 625 grain growth from available literature data is impossible due to the fact that they pertain to Alloy 625 specimens that have been subjected to prior or post heat treatment and/or deformation. That is to say, the disparate initial grain structures/grain boundary areas, precipitate populations and ageing profiles precludes the chance of any reasonable comparison of previously

25 reported data. Under this circumstance it is the unique, and primary objective of this work to analyse the effect of concomitant precipitate formation on the grain evolution of solution annealed Alloy 625.

2. Experimental Program

In order to capture the effect of principally both γ'' and δ phase, but also carbide phases,

30 ageing of the material was performed at temperatures between 600-800°C for durations of up to 3000 hours. Such conditions were selected on the basis of the TTT curve published for Alloy 625 by Floreen *et al.*, an adapted (temperatures in degrees Celsius) version of which is shown in Figure 1. To ensure uniformity between samples, each was solution annealed prior to ageing through heating to 1150°C and holding for 30 minutes (based on

35 the curves of Floreen *et al.* and others [22, 23], and due to its successful demonstration by Shankar *et al.* [9] to dissolve all precipitates except some primary carbides) before being quenched into water. Similarly, following ageing, microstructural evolution was stopped through immediately quenching the sample into water. Through the analysis of successive ageing times both the effect of the growth and coarsening of γ'' precipitates and their ultimate

40 replacement by their thermodynaimcally stable counterpart phase δ can be inferred. This latter phenomenon is widely known to adversely effect the strength of the alloy due to the

3

elimination of the coherency between the matrix and precipitate phase [20, 24].
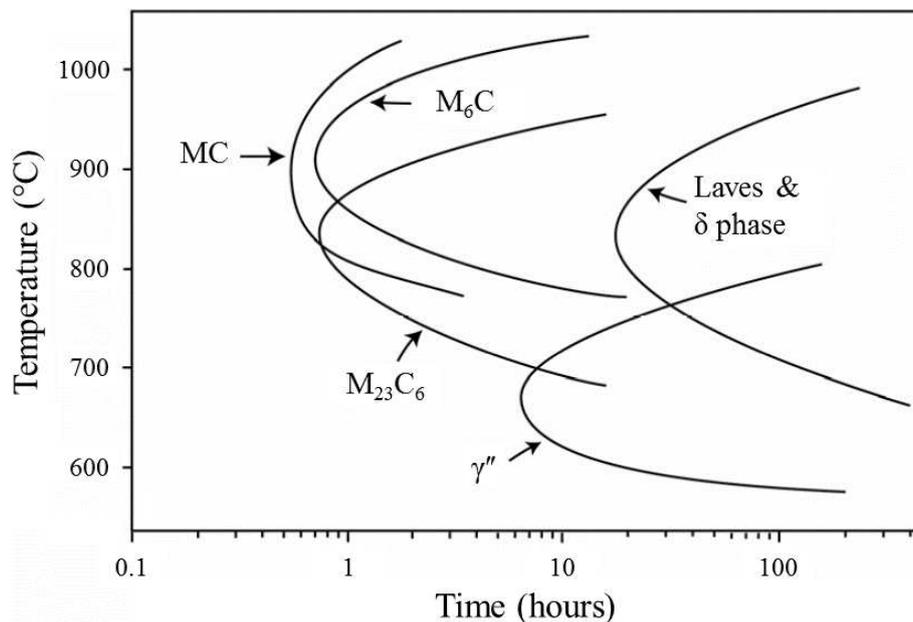
Figure 1: Schematic Time-Temperature-Transformation (TTT) diagram for solution annealed, wrought Alloy 625. Adapted from Floreen *et al.* [25]

The composition of the Alloy 625 analysed in this investigation is given in Table 1.

Table 1: Alloy 625 composition determined by ICP-OES.

Element	Ni	Cr	Fe	Mo	Nb	C	Mn	Si	P	S	Al	Ti
wt%	bal.	21.74	2.87	8.58	3.80	0.021	0.20	0.23	< 0.01	0.003	0.12	0.16

The method used to reveal the grain structure of the aged Alloy 625 material consisted firstly of grinding and polishing each specimen to a scratch-free finish, utilising a fine $0.06 \mu m$ amorphous colloidal silica suspension for the final stage. Subsequent to this, samples were etched by submerging for a few seconds in a 50:50 hydrochloric acid hydrogen peroxide mix once the solution had begun to vigorously effervesce. Examples of the grain structures captured for an isochronal and an isothermal data set are given in Figure 2.

Quantification of the grain size was performed via the Heyn linear intercept method as outlined in ASTM E112-13 [26] on images taken by and optical microscope. Five images were
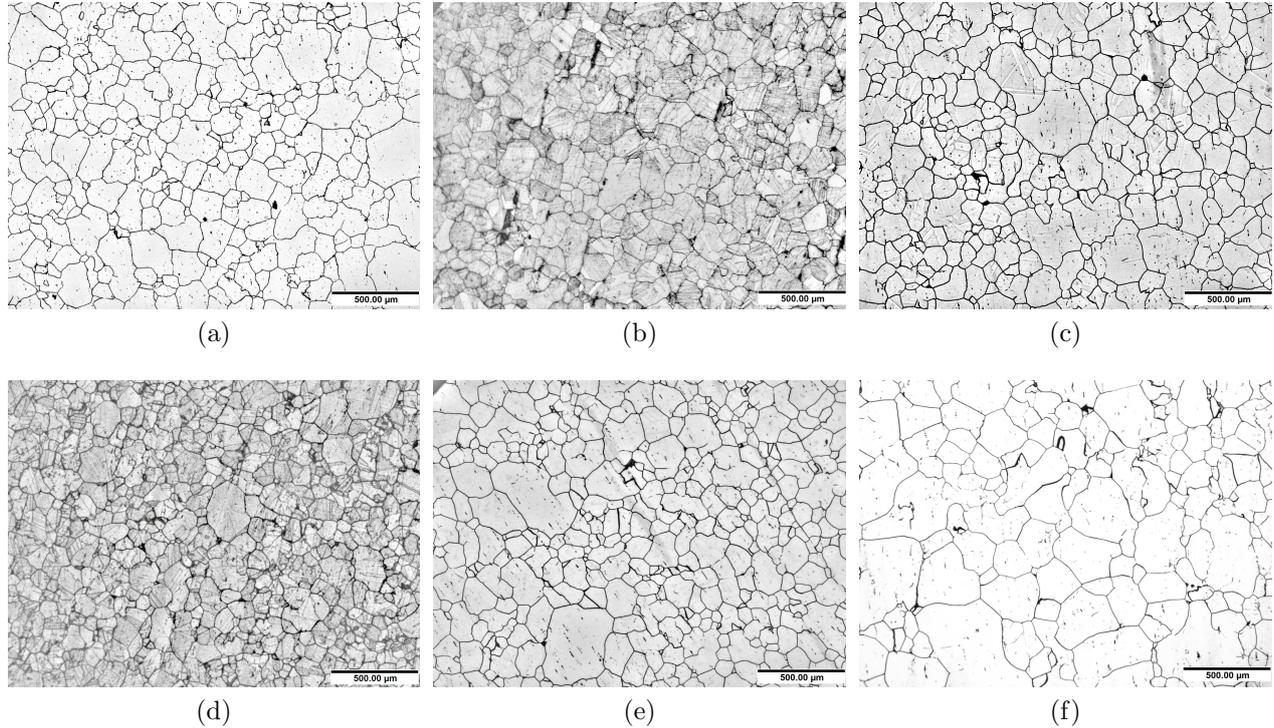
Figure 2: Images of grains revealed in Alloy 625 samples aged for the following durations and temperatures: a) 10 hours at 700°C, b) 50 hours at 700°C, c) 100 hours at 700°C, d) 200 hours at 650°C, e) 200 hours at 700°C, f) 200 hours at 750°C.

analysed for each sample with 5 linear intercept lines used on each image (25 measurements in total per sample). Owing to the correlation between the material hardness and the evolution of the various precipitate phases possible in Alloy 625 [27, 28] (particularly γ''), Vickers hardness testing was performed on polished samples with an automatic Struers DuraScan-80, taking 5 measurements for each sample using a load of 1kg (HV1) and a duration of 60 seconds (due to the high elastic recovery of the alloy). TEM and EDXS analysis later used to identify grain boundary carbides was performed using an FEI Tecnai 20 200 kV Analytical Electron Microscope equipped with an Oxford Instruments Xmax80 Windowless SDD and AZTEC analysis system on foil specimens thinned using Struers Tenupol with a 20% $HClO_4$ 80% ethanol electrolyte.

3. Results and discussion

3.1. Grain Structure

The discovery of an inhomogeneous grain structure across all samples (as imaged in Figure 2) is attributed to the location of the material in the original forging displayed in Figure 3. That it to say, numerous researchers have identified the deformation temperature to have a critical influence on the recrystallization behaviour of Alloy 625 [29, 30, 31, 32], leading to potential significant disparities in the recrystallisation fraction throughout the thickness of products due to thermal gradients [33]. It is, therefore, likely that the lower temperature experienced by the surface adjacent region of the Alloy 625 forging ultimately analysed in this work fell below (owing to both convective/radiative cooling and conduction with the forging press) that which would have been sufficient (depending on the strain rate) to ensure a uniform recrystallisation.
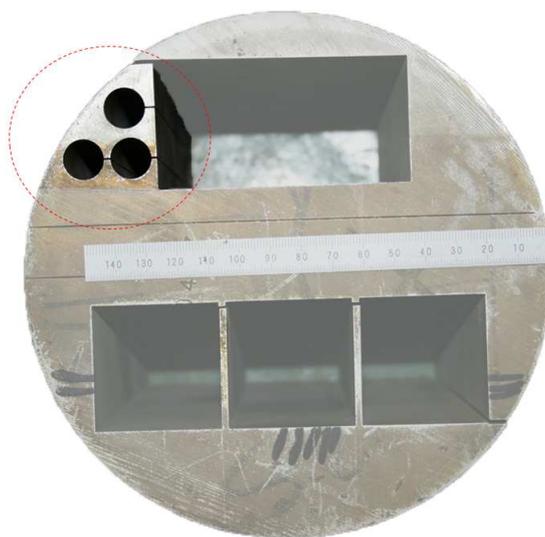
Figure 3: Alloy 625 sample procured from AMEC indicating its original location in Alloy 625 forging. The captured features are the result of Electrical Discharge Machining (EDM), the process of which also caused the observed discolouration/staining of the surface.

As discussed in the subsequent analysis, the ultimate effect of this inhomogeneous grain structure is to introduce a random fluctuation between adjacently cut samples and even

captured images. Nevertheless, given that 1) normal grain growth describes the change in average grain size driven solely by the reduction in grain boundary area [34], 2) that this factor does not directly correlate with average grain size and 3) the in homogeneity appears uniformly randomised across all samples: Calculation of a sufficiently comparable average grain size and change rate across all ageing conditions can be achieved through a sufficient sampling of the inhomogeneous structure such as that performed here. Moreover, given the origin of the grain structure, its analysis constitutes a interesting exercise for anyone concerned with the practical utilisation of Alloy 625 products. The only condition which must be placed on the results is with respect to the specific magnitudes of the variables calculated *e.g.* a homogeneous grain structure will display the same general behaviour but will likely be defined by a slightly different specific activation energy.

3.2. Normal Grain Growth Analysis

The classical expression describing normal isothermal grain growth is given in Equation 1 where $\bar{D}(t)$ is the average grain size at time t, $\bar{D}_0$ is the initial grain size and n and k are exponent and rate constants respectively [34].

$$\bar{D}(t) - \bar{D}_0 = kt^n \tag{1}$$

Treating grain growth as a thermally-activated process, the rate constant k can alternatively be defined by an Arrhenius equation yielding the well known expression in Equation 2, where Q is the apparent activation energy for grain growth, k_2 is a constant dependent on the physical kinetics, R is the ideal gas constant and T is the absolute temperature [35].

$$\bar{D}(t) - \bar{D}_0 = k_2 \exp\left(\frac{-Q}{RT}\right) t^n \tag{2}$$

Following these equations (i.e. assuming normal grain growth), a full description of the grain growth kinetics of Alloy 625 in the temperature range analysed in this study can only be gained through determination of variables n, Q and k_2: n may be found through the fitting of the linearised version of Equation 1 (Equation 3) to isothermal grain size plots, with Q and k_2 subsequently calculated through fitting of Equation 4 to isochronal trends utilising the relevant values for the time exponents. In this study the value of $\bar{D}_0$ is taken from measurements made on a sample subject to the solution annealing treatment only.

$$\ln\left(\bar{D}(t) - \bar{D}_0\right) = \ln(k) + n\ln(t) \tag{3}$$

$$\ln\left(\frac{\bar{D}(t) - \bar{D}_0}{t^n}\right) = \ln(k_2) - \frac{Q}{RT} \tag{4}$$

3.2.1. Time Exponent and TEM analysis of Grain boundary Carbides

Isothermal plots of grain size are shown in Figure 4 together with least squares linear regression fits which also incorporate the uncertainties associated with each datapoint. The resultant values of for the time exponent are given in Table 2. The initial grain size (D_0) of $79.9 \pm 10.9\mu$m was determined from analysis of the solution annealed material and is in agreement with the order of magnitude found by Suave *et al.* [36] for a similar heat treatment of their "as received" material ($56.2\pm28.1\mu$m after 5 minutes at 1090°C). However, the uncertainty in the magnitude of D_0 was excluded from the calculations of subsequent parameters to prevent the production of un-physical results *i.e.* $D_0 > D(t)$. Given its utilisation for the calculation for every data point, it should be pointed out that whilst this truncation of the uncertainty may consequence in a distortion of the specific values of the time exponent, the relative behaviour between isothermal datasets is unaffected.

8

The observation of both reducing n values and is indicative of an increased restriction of grain boundary movement with temperature despite the significant reduction in solute drag which should be experienced in such a heavily alloyed material [37]. Identification of the cause of this phenomenon can be made through comparison to the TTT diagram: Grain boundary carbide precipitates have been shown to significantly impede grain boundary motion and lead to grain refinement in superalloys [38, 39, 40] and from Figure 1 the formation rate (and therefore quantity) of $M_{23}C_6$ and M_6C, which primarily nucleate on grain boundaries in Alloy 625 [41, 42, 43], should increase rapidly from 600-800°C. An illustration of the reverse of this mechanism was given in a recent paper by Suave *et al.* [36] which detailed that the dissolution of M_6C particles in as-received Alloy 625 material led to a substantial increase in the grain growth rate when ageing at temperatures above 900°C.
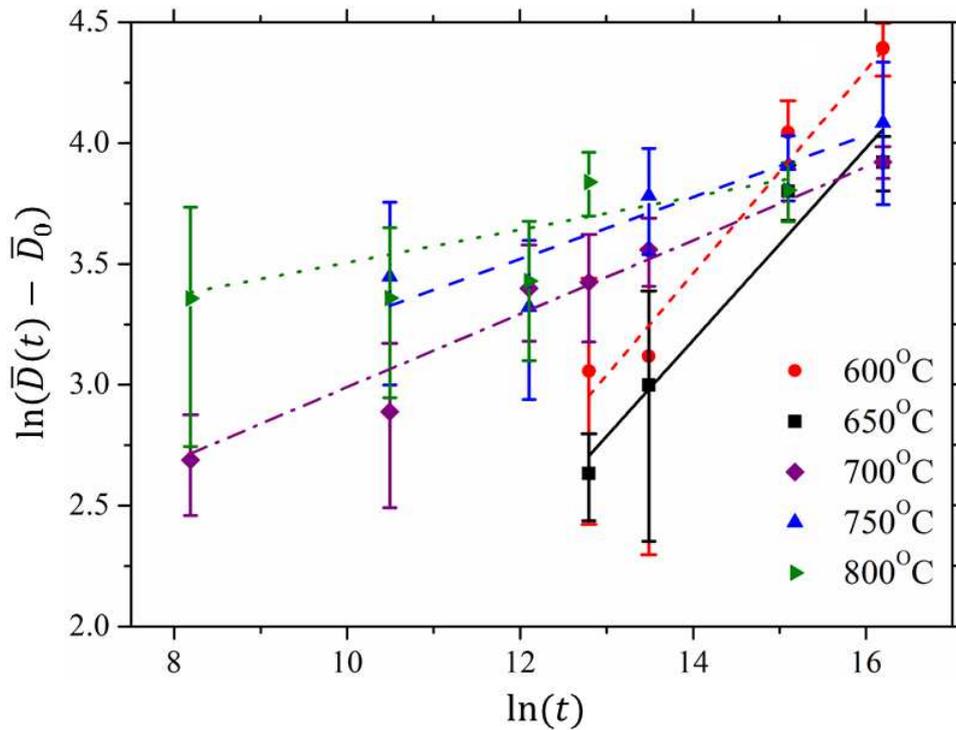
Figure 4: Isothermal grain growth trends for Alloy 625. The grain size D is in units of micrometres and the ageing time t in seconds. Error-bars correspond to one standard deviation about mean grain size values.

Verification of the presence of carbides that could exert such an influence on the grain

9

Table 2: Time exponents calculated from least squares fitting to isothermal grain growth trends.

Temperature (°C)	Time exponent, n
600	0.42 ± 0.07
650	0.40 ± 0.06
700	0.15 ± 0.01
750	0.13 ± 0.03
800	0.07 ± 0.04

evolution of the material examined here is provided by selected area electron diffraction (SAD) patterns acquired via TEM from precipitates formed at $600°C$, $700°C$ and $800°C$ shown in Figures 5a, d and g. These are characteristic of face-centre-cubic (FCC) $M_{23}C_6$ particles obeying a cube-cube ({001}carbide // {001} matrix (<100> carbide // <100> matrix) orientation relationship with the matrix [44]. Furthermore, the high level of chromium measured by EDXS scans of the same particles (Figures 5b, e and f) show the distinctive traits of $M_{23}C_6$ (specifically $Cr_{23}C_6$). The comparatively small enrichment of molybdenum (Figures 5c, f and g) in the same particles is consistent with a the work of Raghavan *et al.* [45] who found a solubility of 10 at.% Mo in $M_{23}C_6$ precipitates in Ni-Cr-Mo alloys irrespective of the Mo concentration. However, areas evidenced to have a higher concentration of Mo are likely to instead be related to M_6C particles *viz.* their increased presence at $800°C$ is in accordance with the TTT curve for the phase displayed in Figure 1.

Lastly, with reference to the time exponent (n) values, the not insignificant magnitude of their associated uncertainties (particularly at 800°C), resulting from scatter in the data points, indicates can attributed to the inhomogeneous initial grain structure described in the previous section.

10
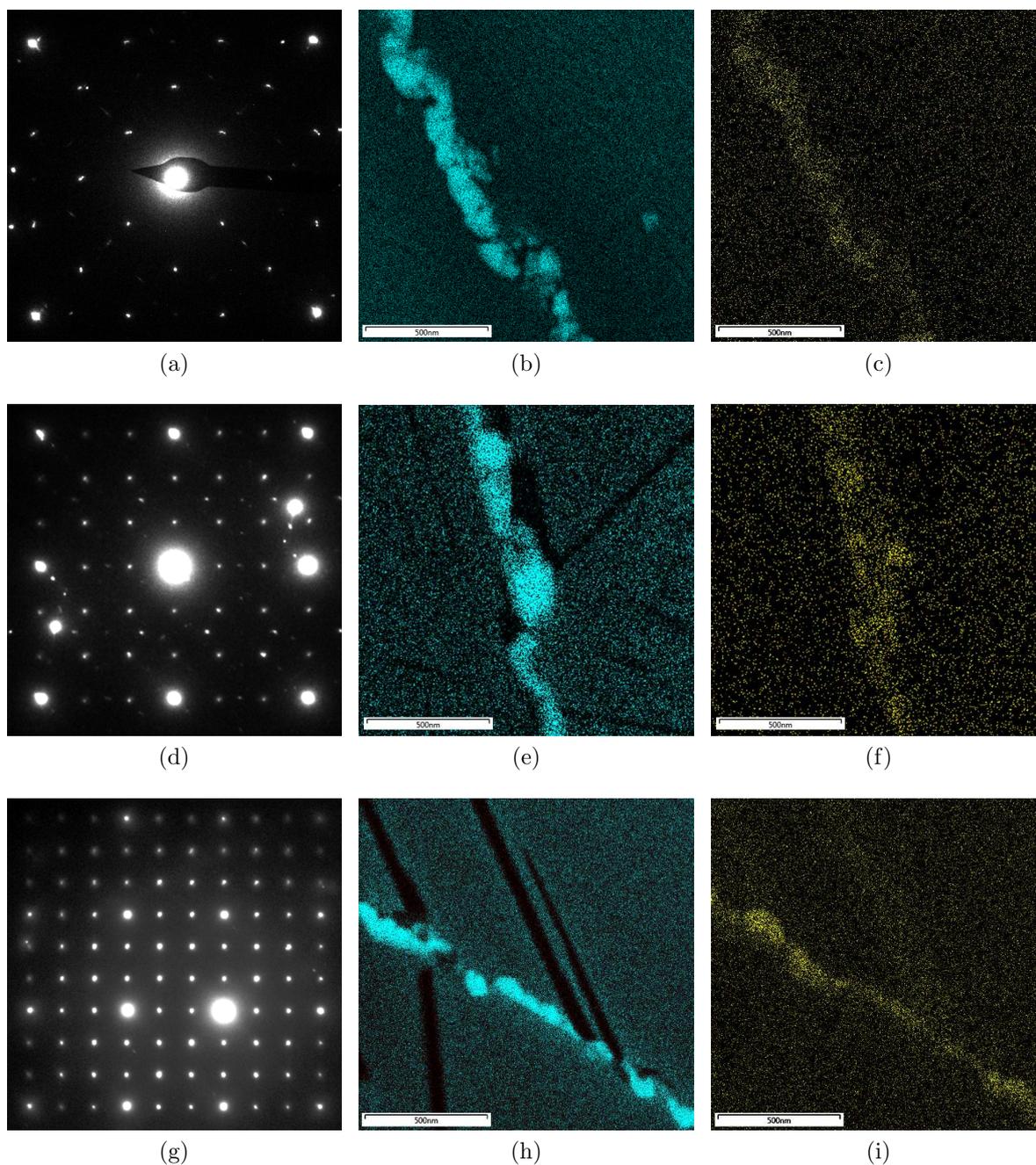
Figure 5: SAD patterns and EDXS scans of grain boundary precipitates in aged Alloy 625 samples. a) [001] orientated SAD pattern, b) Cr K Series scan, c) Mo K Series scan for material aged at 600°C for 3000 hours. d) [001] orientated SAD pattern, e) Cr K Series scan, f) Mo K Series scan for material aged at 700°C for 200 hours. g)[001] orientated SAD pattern, h) Cr K Series scan, i) Mo K Series scan for material aged at 800°C for 200 hours.

3.2.2. Activation energy and rate constant

With the value of n determined for each temperature, isochronal plots corresponding to the relation detailed in Equation 4 can be created as shown in Figure 6. It is immediately noticeable from the data points that at least two distinct growth regime regions exist for the alloy, one incorporating temperatures around 600-650°C and another around temperatures of 700-800°C. As consequence, rather than making a singular fit to the entire data set two separate fits, one for each of these regions, are made instead as indicated in the figure. The values for the activation energy and rate constant calculated accordingly for each region, together with a separate trend inferred from the intervening temperatures, are listed in Table 3.
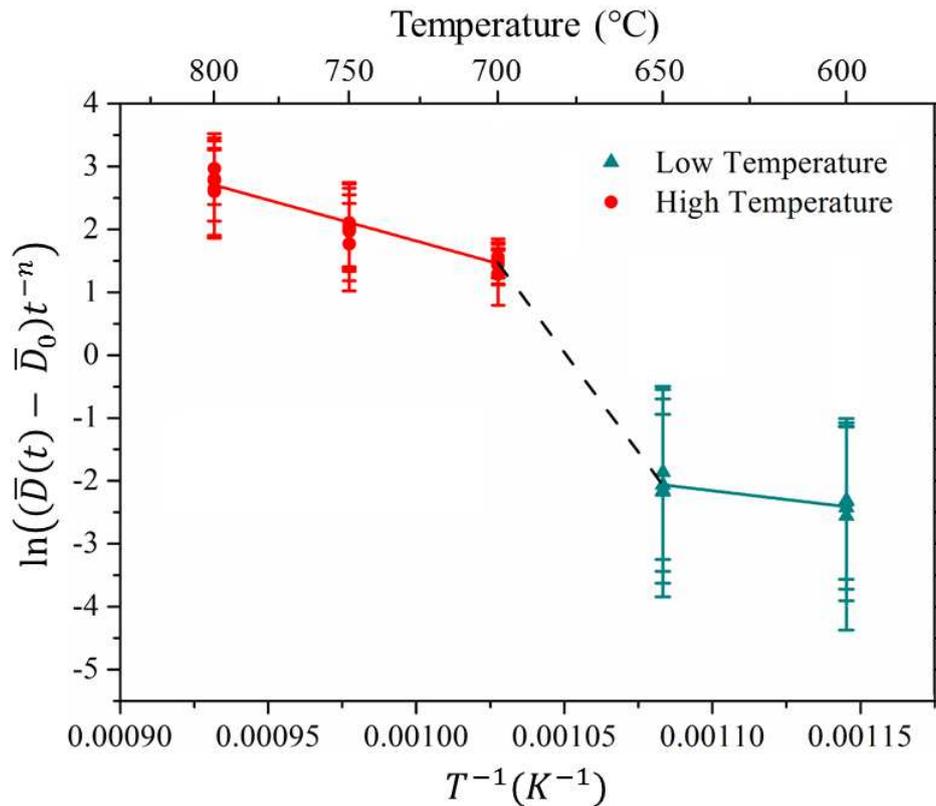
Figure 6: Isochronal grain growth trends for Alloy 625. High and low temperature growth regime regions are indicated. Error-bars correspond to a combination of one standard deviation about mean grain size values and that calculated for n in Table 2.

Table 3: Activation energy and rate constant calculated from least squares fitting to average isochronal grain growth trends.

Temperature Range (°C)	Activation energy, Q (kJ mol^{-1})	Rate Constant, k_2
600-650	46.6 ± 12.2	55^{+228}_{-44}
650-700	527.7 ± 23.1	$0.1^{+1.6}_{-0.1} \times 10^{30}$
700-800	108.3 ± 6.6	$1.8^{+9.7}_{-1.5} \times 10^{6}$

Comparison of the trends obtained here to those developed by Cahn [46, 37], based on the theoretical treatment of the effects of solute drag, allows one to conclude the seeming three regime behaviour is a manifestation of a so called intermediate or high driving force mechanism for grain boundary migration operating within the alloy. That is, the driving force is of sufficient magnitude for the grain boundary to reach high enough velocities where the transition between the impure (solute drag increasing with velocity) and pure (solute drag decreasing with velocity) type boundary movement expected with temperature in the alloyed system is defined by an inflection.

The particularly high solute concentration in Alloy 625, means the probability of the system operating specifically in the high driving force regime, whereby the calculation leads to the formation of an unstable region in which the slope theoretically becomes negative, is significant. As a result, rather than a high activation energy transitional region as indicated in Figure 6, a discontinuous transition between the high and low velocity regions is most likely [46, 37]. However, due to the narrowness of the inflection region, conclusive discrimination between either the intermediate or high driving force schemes existing within the alloy can only be achieved through the gathering of additional experimental data in the relevant temperature range (*i.e.* 650-700°C).

With regard to the specific vales detailed in Table 3 for Alloy 625, the activation energy for volume self-diffusion in Alloy 625 calculated as a weighted average from binary couples detailed in the literature [47, 48, 49, 50] is estimated as 148.6 kJ mol^{-1}. Accordingly, as

13

the activation energy for grain boundary diffusion in nickel is typically around half that in the bulk [49] it is likely gain boundary diffusion which is the principle (*i.e.* subject to the aforementioned influence of solute drag and, separately, grain boundary/ interface diffusion) governing mechanism for grain growth over both the upper and lower temperature regimes [51]. The value of $Q = 527.7 \pm 23.1$ kJ mol^{-1} calculated for the intermediate region through linear extrapolation between 650-700°C is only appropriate if the system generates just an intermediate driving force for grain boundary motion and, even in such an instance, is subject to change with the gathering of more experimental data.

3.2.3. Vickers Hardness

Vickers hardness plots measured from aged samples are shown in Figure 7. According to the Hall-Petch relationship [52, 53], a reduction in hardness is expected as the grain structure of material coarsens, but such a trend is not observed over any of the measured conditions for Alloy 625 here. Instead, comparison of the trends with a number of different TTT curves detailed in the literature for Alloy 625, as per Figure 9, enables the conclusion that it is intermetallic precipitates which produce the observed hardening, with γ'' particles overwhelmingly having the greatest impact. The significant strengthening imparted by γ'' precipitates has been noted by many researchers [7, 8, 9, 10, 54, 55], however the results here also imply that even a wide spread δ phase population (as evidenced directly by the optical micrograph in Figure 8) is still more than sufficient overcome the deleterious effect of increasing average grain size despite its much poorer strengthening properties compared to γ'' [20].

In addition to the above conclusions, the relationships presented in Figure 7 also allow one to infer some of the evolutions of the intermetallic precipitates occurring in the material during heat treatment. Specifically, the observance of a cross over in the hardness values of material aged at 600°C versus that aged at 650°C after 3000 hours indicates that the precipitate size distribution has coarsened significantly and a likely transformation to δ phase

14
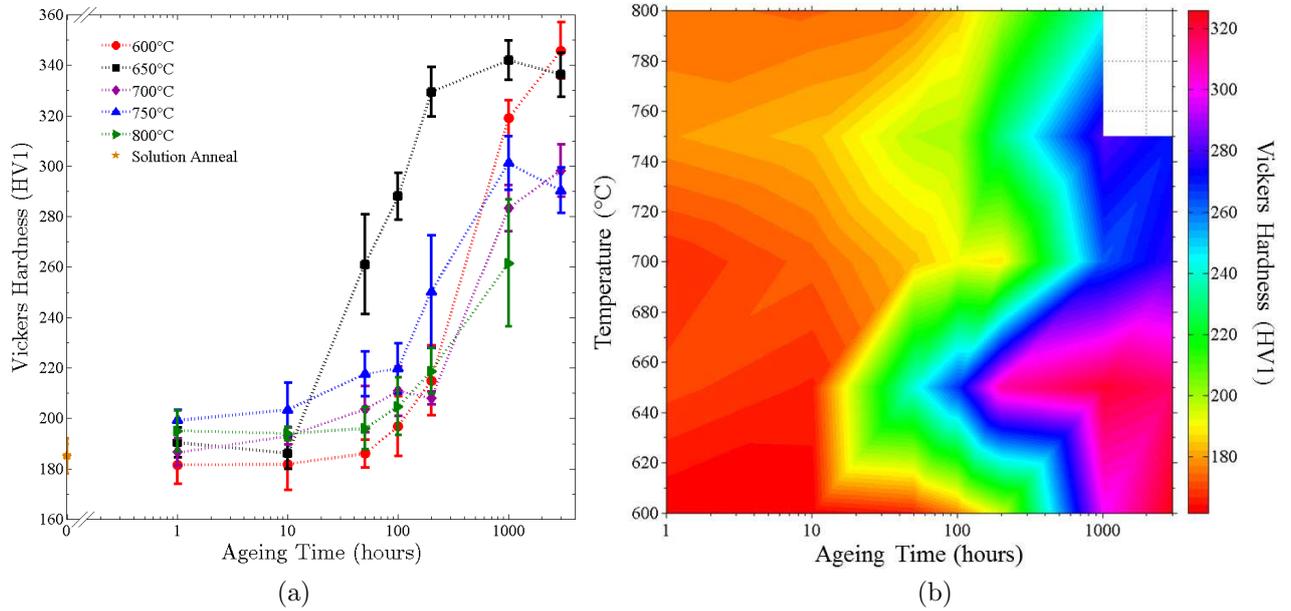
Figure 7: a) Vickers hardness plot and b) Vickers hardness surface generated from linear interpolation between measurements made on aged Alloy 625 specimens. Error-bars correspond to 1 standard deviation about the mean value. It is worth noting that comparison of the average indent size of 7-10μm with the range of grain sizes 90-140μm means the hardness measurements were almost certainly taken exclusively from intra granular regions and are therefore not subject to random grain boundary influences.

has initiated at the higher temperature due to only the latter phase being thermodynamically stable [56]. In contrast, an opposite temperature behaviour is seen between 700°C and 750°C reflecting the shape of the TTT curves for the γ'' phase. The substantial hardening seemingly imparted by δ phase (*cf.* Figure 9) at temperatures $\geq$ 750°C constitutes a validation of the detection of the same phenomenon by Suave *et al.* [27]. It is worth noting that as only the envelope of the γ'' produced by Floreen *et al.* corresponds well with the hardening response observed here over the full temperature range, this research suggests that use of Figure 1 as common reference for the likely response of an Alloy 625 specimen is appropriate.

The fact that intermetallic precipitates are detected but that no discernible correlation is observed be between the results in Figure 7 and those for grain size in Figure 4 is a significant result as it provides further evidence for the conclusion that it is carbides which

15
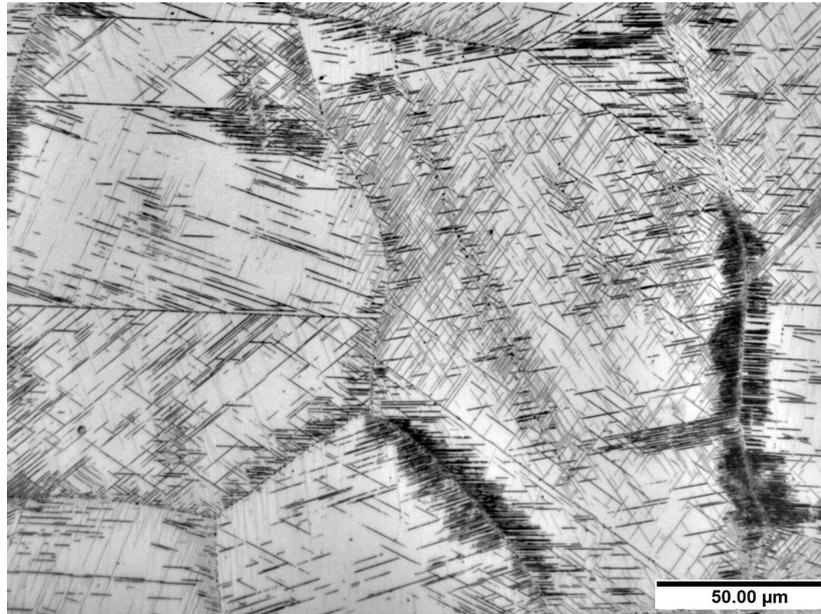
Figure 8: Optical micrograph showing needle like δ phase precipitates in a sample of Alloy 625 aged for 3000 Hours at 700°C and etched with a 50:50 hydrochloric acid hydrogen peroxide mix.

are the dominant precipitate phase in terms of the control the grain evolution of Alloy 625. That is, assuming the counterfactual, given the hardening results one would expect to see a likely oscillatory behaviour grain size about a minima at 650°C where the more rapidly formed and larger phase fraction of γ'' would restrict the grain growth most severely.

4. Summary and Conclusions

Measurements of grain size carried out on samples of Alloy 625 likely to contain precipitates have indicated the process to be dominated by both grain boundary carbide precipitation and solute drag. The influence of the former of these two phenomena is evident principally in the evolution of the time exponent in the normal grain growth equation, with the increased Zener pinning pressure exerted by grain boundary nucleated particles leading to a reduction in the parameter with temperature. The accompanying effect of solute drag on grain boundary motion is identified from the temperature dependence of grain boundary velocity. Specifically, following the work of Cahn [57] the establishment of two behavioural

16
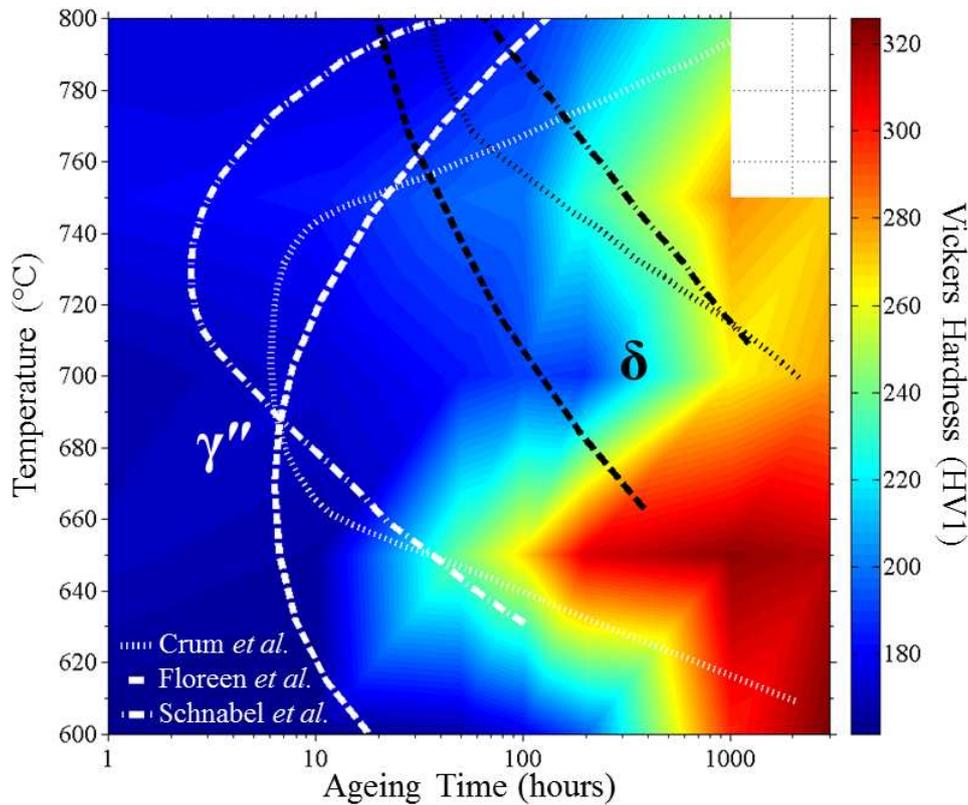
Figure 9: Vickers hardness surface generated from measurements made on aged Alloy 625 specimens overlayed with the γ'' and δ phase TTT curves produced by Floreen *et al.* [25] (Figure 1) Crum *et al.* [23] and Schnabel *et al.* [22]. Line colours indicate the precipitate phase type and line dashes the literature source.

regions allows a high driving force and high solute mechanism to be inferred. These findings are consistent with the previously established TTT diagram for the alloy and the high levels of solute atoms ($> 30\%$) present within it.

The activation energies for grain growth of the relatively inhomogeneous samples in the low and high temperature regions were calculated as 46.6 ± 12.2kJ mol^{-1} and 108.3 ± 6.6 kJ mol^{-1} respectively. Comparison of these values with activation energy for volume self-diffusion identifies grain boundary diffusion to be the principle growth mechanism in both instances. The existence of a high activation energy (indicatively calculated here as 527.7 ± 23.1 kJ mol^{-1}) or discontinuous jump in transitional region for boundary velocity, associated with an intermediate or high driving force mechanism respectively, requires further investigation.

17

The presence of intermetallic precipitates was detected by Vickers hardness testing, with their behaviour corresponding most strongly to the TTT diagram of Floreen et al. [25]. However, no correlation was found between their emergence and evolution in Alloy 625 and the grain growth and coarsening behaviour. This result provides key evidence for carbides being the controlling precipitate phase with respect to the grain size of the alloy.

Acknowledgements

References

[1] J. Davis, Heat-Resistant Materials, ASM Specialty Handbook, ASM International, Metals Park, OH, 1997.

[2] G. Smith, S. Kiser, J. Crum, C. Tassen, Nickel base alloys improve corrosion resistance, The International Journal of Hydrocarbon Engineering 5 (2) (1999) 7.

[3] D. Capitanescu, Alloy 625 weld overlays for offshore and onshore projects, in: E. Loria (Ed.), Proceedings of the International Symposium on Superalloys 718, 625 and Various Derivatives, The Minerals, Metals & Materials Society, Warrendale, PA, 1991, pp. 821–835.

[4] M. Kutz, Handbook of Materials Selection, John Wiley & Sons, Inc., 2002.

[5] J. Crum, G. Smith, H. Flower, Resistance of Automotive Exhaust Flexible Coupling Alloys to Hot Salt Attack, Stress Corrosion Cracking and High Temperature Embrittlement, SAE Technical Paper 1999-01-0372.

[6] E. P. R. Institute, Critical Issues Report and Roadmap for the Advanced Radiation-Resistant Materials Program, http://www.epri.com/abstracts/Pages/ProductAbstract.aspx?ProductId=000000000001026482.

[7] J. Oblak, D. Paulonis, D. Duvall, Coherency strengthening in Ni base alloys hardened by D0$_{22}$ γ'' precipitates, Metallurgical Transactions 5 (1974) 143–153.

[8] B. Hyatt, C. Brown, Microstructure and mechanical properties of stress relieved electron beam welded Alloy 625, in: E. Loria (Ed.), Proceedings of the International Symposium on Superalloys 718, 625, 706 and Various Derivatives, Vol. 1, The Minerals, Metals & Materials Society, Warrendale, PA, 2001, pp. 645–656.

[9] V. Shankar, K. Bhanu Sankara Rao, S. Mannan, Microstructure and mechanical properties of Inconel 625 superalloy, Journal of Nuclear Materials 288 (2-3) (2001) 222–232.

[10] M. Shaikh, M. Ahmad, K. Shoaib, J. Akhter, M. Iqbal, Precipitation hardening in Inconel * 625, Materials Science and Technology 16 (2) (2000) 129–132.

[11] M. Burke, W. Mills, R. Bajaj, Microstructure and properties of direct-aged Alloy 625, in: E. Loria (Ed.), Proceedings of the International Symposium on Superalloys 718, 625, 706 and Various Derivatives, Vol. 1, The Minerals, Metals & Materials Society, Warrendale, PA, 2001, pp. 389–398.

[12] J. Chakravartty, J. Singh, M. Sundararaman, Microstructural and mechanical properties of service exposed Alloy 625 ammonia cracker tube removed after 100 000h, Materials Science and Technology 28 (6) (2012) 702–710.

[13] M. Köhler, Effect of the elevated-temperature-precipitation in Alloy 625 on properties and microstructure, in: E. Loria (Ed.), Proceedings of the International Symposium on Superalloys 718, 625 and Various Derivatives, The Minerals, Metals & Materials Society, Warrendale, PA, 1991, pp. 363–374.

[14] The performance of Alloy 625 in long-term intermediate temperature applications, International Journal of Pressure Vessels and Piping 59 (1-3) (1994) 41 – 49.

[15] M. Sundararaman, P. Mukhopadhyay, S. Banerjee, Influence of intermetallic phase precipitation during prolonged service in Alloy 625 on its properties, in: E. Loria (Ed.), Proceedings of the International Symposium on Superalloys 718, 625, 706 and Various Derivatives, The Minerals, Metals & Materials Society, Warrendale, PA, 2001, pp. 367–378.

[16] J. Radavich, A. Fort, Effects of long-time exposure in Alloy 625 at 1200°F 1400°F and 1600°F, in: E. Loria (Ed.), Proceedings of the International Symposium on Superalloys 718, 625, 706 and Various Derivatives, The Minerals, Metals & Materials Society, Warrendale, PA, 1994, pp. 635–647.

[17] H. Pai, M. Sundararaman, A comparison of the precipitation kinetics of γ'' particles in virgin and re-solutioned Alloy 625, in: E. Loria (Ed.), Proceedings of the International Symposium on Superalloys 718, 625, 706 and Various Derivatives, The Minerals, Metals & Materials Society, Warrendale, PA,

2005, pp. 487–495.

[18] J. Mittra, S. Banerjee, R. Tewari, G. Dey, Fracture behavior of Alloy 625 with different precipitate microstructures, Materials Science and Engineering A 574 (2013) 86–93.

[19] M. Ahmad, W. Ahmad, M. Shaikh, M. Ahmad, M. Rajput, Precipitation study in Inconel 625 Alloy by positron annihilation spectroscopy, Journal of Materials Science and Technology 19 (5) (2003) 434–436.

[20] C. Sims, N. Stoloff, W. Hagel, Superalloys II, 1st Edition, Wiley, New York, USA, 1987.

[21] H. Eiselstein, D. Tillack, The invention and definition of Alloy 625, in: E. Loria (Ed.), Proceedings of the International Symposium on Superalloys 718, 625 and Various Derivatives, The Minerals, Metals & Materials Society, Warrendale, PA, 1991, pp. 1–14.

[22] E. Schnabel, H. Schueller, P. Schwaab, Precipitation and recrystallization behavior of the nickel- base alloy Inconel 625, (das ausscheidungs- und rekristallisationsverhalten der nickelbasislegierung Inconel 625), Praktische Metallographie/Practical Metallography 8 (9) (1971) 521–527.

[23] J. Crum, M. Adkins, W. Lipscomb, Performance of high nickel alloys in refinery and petrochemical environments., Materials Performance 25 (7) (1986) 27–33.

[24] R. C. Reed, The Superalloys: Fundamentals and Applications, 1st Edition, Cambridge University Press, Cambridge, UK, 2006.

[25] S. Floreen, G. Fuchs, W. Yang, The metallurgy of Alloy 625, in: E. Loria (Ed.), Proceedings of the International Symposium on Superalloys 718, 625, 706 and Various Derivatives, The Minerals, Metals & Materials Society, Warrendale, PA, 1994, pp. 13–37.

[26] ASTM International, ASTM E112-13, Standard Test Methods for Determining Average Grain Size, West Conshohocken, PA (2013).

[27] L. Suave, D. Bertheau, J. Cormier, P. Villechaise, A. Soula, Z. Hervier, F. Hamon, J. Laigo, Impact of thermomechanical aging on Alloy 625 high temperature mechanical properties, in: E. Ott, A. Banik, X. Liu, I. Dempster, K. Heck, J. Andersson, J. Groh, T. Gabb, R. Helmink, A. Wusatowska-Sarnek (Eds.), Proceedings of the 8th International Symposium on Superalloy 718 and Derivatives, John Wiley & Sons, Inc., Hoboken, NJ, 2014, pp. 317–331.

[28] S. Mannan, F. Veltry, Time-Temperature-Transformation diagram of Alloy 725, in: E. Loria (Ed.), Proceedings of the International Symposium on Superalloys 718, 625, 706 and Various Derivatives, Vol. 1, The Minerals, Metals & Materials Society, Warrendale, PA, 2001, pp. 345–356.

[29] L. Ferrer, B. Pieraggi, J. Uginet, Microstructural evolution during thermomechanical processing of Alloy 625, in: E. Loria (Ed.), Proceedings of the International Symposium on Superalloys 718, 625 and

20

320 Various Derivatives, The Minerals, Metals & Materials Society, Warrendale, PA, 1991, pp. 217–228.

[30] D. Zhao, P. Chaudhury, R. Frank, L. Jackman, Flow behavior of three 625 type alloys during high temperature deformation, in: E. Loria (Ed.), Proceedings of the International Symposium on Superalloys 718, 625, 706 and Various Derivatives, The Minerals, Metals & Materials Society, Warrendale, PA, 1994, pp. 315–329.

325 [31] S. Guo, D. Li, Q. Guo, Z. Wu, H. Peng, J. Hu, Investigation on hot workability characteristics of Inconel 625 superalloy using processing maps, Journal of Materials Science 47 (15) (2012) 5867–5878.

[32] B. López, J. Urcola, Hot deformation characteristics of Inconel 625, Materials Science and Technology 12 (8) (1996) 673–678.

[33] D. Camus, R. Jaramillo, J. Plybum, F. Suarez, Evolution of microstructure during hot rolling of Inconel
330 alloys 625 and 718, in: E. Loria (Ed.), Proceedings of the International Symposium on Superalloys 718, 625, 706 and Various Derivatives, The Minerals, Metals & Materials Society, Warrendale, PA, 1997, pp. 291–302.

[34] B. Ralph, Grain growth, Materials Science and Technology 6 (11) (1990) 1136–1144.

[35] P. Cotterill, P. Mould, Recrystallization and grain growth in metals, Surrey University Press, Guildford,
335 UK, 1976.

[36] L. Suave, J. Cormier, P. Villechaise, A. Soula, Z. Hervier, D. Bertheau, J. Laigo, Microstructural evolutions during thermal aging of Alloy 625: Impact of temperature and forming process, Metallurgical and Materials Transactions A: Physical Metallurgy and Materials Science 45 (7) (2014) 2963–2982.

[37] G. T. Higgins, Grain-boundary migration and grain growth, Metal Science 8 (1) (1974) 143–150.

340 [38] S. Xu, J. Dickson, A. Koul, Grain growth and carbide precipitation in superalloy, Udimet 520, Metallurgical and Materials Transactions A: Physical Metallurgy and Materials Science 29 (11) (1998) 2687–2695.

[39] G. Smith, S. Patel, The role of niobium in wrought precipitation-hardened nickel-base alloys, in: E. Loria (Ed.), Proceedings of the International Symposium on Superalloys 718, 625, 706 and Various Derivatives, The Minerals, Metals & Materials Society, Warrendale, PA, 2005, pp. 135–154.

[40] L. Jackman, M. Boldy, A. Coffey, The influence of reduced carbon on Alloy 718, in: E. Loria (Ed.), Proceedings of the International Symposium on Superalloys 718, 625 and Various Derivatives, The Minerals, Metals & Materials Society, Warrendale, PA, 1991, pp. 261–270.

[41] C. Vernot-Loier, F. Cortial, Influence of heat treatments on microstructure, mechanical properties
350 and corrosion behaviour of Alloy 625 forged rod, in: E. Loria (Ed.), Proceedings of the International

21

Symposium on Superalloys 718, 625 and Various Derivatives, The Minerals, Metals & Materials Society, Warrendale, PA, 1991, pp. 409–422.

[42] J. Corrieu, C. Vemot-Loier, F. Cortial, Influence of heat treatments on corrosion behaviour of Alloy 625 forged rod, in: E. Loria (Ed.), Proceedings of the International Symposium on Superalloys 718, 625, 706 and Various Derivatives, The Minerals, Metals & Materials Society, Warrendale, PA, 1994, pp. 795–806.

[43] M. Sundararaman, P. Mukhopadhyay, S. Banerjee, Carbide precipitation in nickel base superalloys 718 and 625 and their effect on mechanical properties, in: E. Loria (Ed.), Proceedings of the International Symposium on Superalloys 718, 625, 706 and Various Derivatives, Vol. 1, The Minerals, Metals & Materials Society, Warrendale, PA, 1997, pp. 367–378.

[44] X. Dong, X. Zhang, K. Du, Y. Zhou, T. Jin, H. Ye, Microstructure of carbides at grain boundaries in nickel based superalloys, Journal of Materials Science and Technology 28 (11) (2012) 1031–1038.

[45] M. Raghavan, R. Mueller, C. Klein, G. Vaughn, Carbides in Ni-Cr-Mo system, Scripta Metallurgica 17 (10) (1983) 1189–1194.

[46] J. Cahn, The impurity-drag effect in grain boundary motion, Acta Metallurgica 10 (9) (1962) 789–798.

[47] M. Karunaratne, D. Cox, R. Reed, Modelling of the microsegregation in CMSX-4 superalloy and its homogenisation during heat treatment, in: T. Pollock, R. Kissinger, K. Green, M. McLean, S. Olson, J. Schirra (Eds.), Superalloys 2000 (Proceedings of the Ninth International Symposium on Superalloys), The Minerals, Metals & Materials Society, Warrendale, PA, 2000, pp. 263–272.

[48] M. Karunaratne, R. Reed, Interdiffusion of niobium and molybdenum in nickel between 900 - 1300°C, Defect and Diffusion Forum 237-240 (PART 1) (2005) 420–425.

[49] A. Wazzan, Lattice and grain boundary self-diffusion in nickel, Journal of Applied Physics 36 (11) (1965) 3596–3599.

[50] V. Ganesan, V. Seetharaman, V. Raghunathan, Interdiffusion in the nickel-iron system, Materials Letters 2 (4 PART A) (1984) 257–262.

[51] A. Jankowski, J. Ferreira, J. Hayes, Activation energies of grain growth mechanisms in aluminum coatings, Thin Solid Films 491 (1-2) (2005) 61–65.

[52] E. Hall, The deformation and ageing of mild steel: III Discussion of results, Proceedings of the Physical Society. Section B 64 (9) (1951) 747–753.

[53] N. Petch, The cleavage strength of polycrystals, Journal of the Iron and Steel Institute 174 (1953) 25–28.

[54] I. Kirman, D. Warrington, The precipitation of Ni$_3$Nb phases in a Ni-Fe-Cr-Nb alloy, Metallurgical Transactions 1 (10) (1970) 2667–2675.

[55] D. Paulonis, J. Oblak, D. Duvall, Precipitation in nickel-base Alloy 718, ASM-Trans 62 (3) (1969) 611–622.

[56] M. Sundararaman, P. Mukhopadhyay, S. Banerjee, Precipitation of the δ Ni$_3$Nb phase in two nickel base superalloys, Metallurgical Transactions A 19 (3) (1988) 453–465.

[57] R. Cahn, P. Siemers, J. Geiger, P. Bardhan, The order-disorder transformation in ni$_3$al and ni$_3$(al,fe) alloys I. determination of the transition temperatures and their relation to ductility, Acta Metallurgica 35 (11) (1987) 2737–2751.

23